Materials Today Chemistry 35 (2024) 101848

Contents lists available at ScienceDirect

Materials Today Chemistry

journal homepage: www.journals.elsevier.com/materials-today-chemistry/

PEtOxylated polyesteramide nanoparticles for the delivery of anti-inflammatory drugs

Mira Behnke [a,b,1], Antje Vollrath [a,b,1], Philipp Dahlke [c], Francisco Páez Larios [d,e], Mingzhe Chi [f], Ekaterina Tsarenko [a,b], Paul M. Jordan [b,c], Christine Weber [a,b], Michael Dirauf [a,b], Justyna Anna Czaplewska [a,b], Baerbel Beringer-Siemers [a,b], Steffi Stumpf [a,b], Carolin Kellner [a,b], Christian Kretzer [c], Stephanie Hoeppener [a,b], Ivo Nischang [a,b,g,h], Marek Sierka [b,f], Christian Eggeling [b,d,e], Oliver Werz [b,c], Ulrich S. Schubert [a,b,h,*]

[a] Laboratory of Organic and Macromolecular Chemistry (IOMC) Friedrich Schiller University Jena, Humboldtstraße 10, 07743, Jena, Germany
[b] Jena Center for Soft Matter (JCSM) Friedrich Schiller University Jena, Philosophenweg 7, 07743, Jena, Germany
[c] Department of Pharmaceutical/Medicinal Chemistry, Institute of Pharmacy Friedrich Schiller University Jena, Philosophenweg 14, 07743, Jena, Germany
[d] Leibniz Institute of Photonic Technology, Albert-Einstein-Straße 9, 07745, Jena, Germany
[e] Institute of Applied Optics and Biophysics, Friedrich Schiller University Jena, Max-Wien Platz 1, 07743, Jena, Germany
[f] Otto Schott Institute of Materials Research (OSIM), Friedrich Schiller University Jena, Löbdergraben 32, 07743, Jena, Germany
[g] Helmholtz-Zentrum Berlin für Materialien und Energie GmbH (HZB), Hahn-Meitner-Platz 1, 14109 Berlin, Germany
[h] Helmholtz Institute for Polymers in Energy Applications Jena (HIPOLE Jena), Lessingstraße 12-14, 07743, Jena, Germany

ARTICLE INFO

Keywords:
Poly(ester amide)s
Anti-inflammatory drugs
BRP-187
BRP-201
High-throughput nanoparticle formulation
Drug encapsulation
Atomistic molecular dynamics simulations
5-LOX

ABSTRACT

Poly(ester amide)s (PEAs) consisting of L-valine (Val), glycolic acid (G), and L-isoleucine (Ile), *i.e.*, PValG and PIleG, and various poly(2-ethyl-2-oxazoline)-*block*-poly(ester amide) copolymers (PEtOx-*b*-PEA) were investigated for their suitability as particle-based delivery systems for the anti-inflammatory drugs BRP-187 and BRP-201. A small-scale, high-throughput formulation approach was utilized to evaluate the nanoparticle properties in dependence of the composition of mixtures of PEA homo- and copolymers. Atomistic molecular dynamics simulations of PValG and PIleG with the active ingredients indicated thermodynamic compatibility of the PEAs with the drugs. Drug encapsulation studies confirmed the formation of stable formulations, and the enzymatic degradation of the nanoparticles was also demonstrated. The nanoparticles exhibited no cytotoxicity and were able to efficiently deliver the active pharmaceutical ingredients, *i.e.*, BRP-187 and BRP-201 into macrophages and HEK293 cells. All nanoparticle systems displayed anti-inflammatory effectiveness as they were able to suppress cellular 5-lipoxygenase activity. The most promising effects were obtained with the block copolymer-based PEtOx-*b*-PEA nanoparticles, which revealed an enhanced performance compared to the control PLGA nanoparticles.

1. Introduction

Polymer-based nanoparticles have emerged as a promising drug delivery platform due to their versatility and ability to overcome the limitations of free drugs, such as poor bioavailability, rapid clearance from the body, and toxicity [1–3]. Poly(lactic acid) (PLA) and, in particular, the copolymer poly(lactic-*co*-glycolic acid) (PLGA) are typical polymers used for drug delivery applications and, thus, for the formulations of active pharmaceutical ingredients (APIs) [4]. These polymers have a rather hydrophobic character and form the core of the formulated nanoparticle that embeds the API. PLGA is soluble in many organic solvents, but also has a versatile use in applications demanding high biocompatibility. Drawbacks of PLGA include the limited tuning ability of the nanoparticles, *e.g.*, regarding API encapsulation capacities and the occurrence of free drug precipitates in addition to the nanoparticles, as shown in previous studies [5,6]. The latter may be due to

* Corresponding author. Laboratory of Organic and Macromolecular Chemistry (IOMC) Friedrich Schiller University Jena, Humboldtstraße 10, 07743, Jena, Germany.
E-mail address: ulrich.schubert@uni-jena.de (U.S. Schubert).
[1] Authors contributed equally to the study.

https://doi.org/10.1016/j.mtchem.2023.101848
Received 3 October 2023; Received in revised form 29 November 2023; Accepted 6 December 2023
Available online 27 December 2023
2468-5194/© 2023 The Authors. Published by Elsevier Ltd. This is an open access article under the CC BY-NC-ND license (http://creativecommons.org/licenses/by-nc-nd/4.0/).

the presence of only ester functionalities in PLGA, which might cause unfavorable drug-polymer interactions.

Poly(ester amide)s (PEAs) represent a promising alternative class of polymers compared to PLGA. They possess additional amide moieties, which can promote hydrogen bonding, either between the polymer and the API or polymer and polymer, thereby affecting encapsulation of APIs and the biodegradability [7,8]. PEAs obtained from ring-opening polymerization of morpholine-2,5-diones are often referred to as polydepsipeptides. They feature a structure that is very similar to PLGA (Fig. 1) [9,10]. PLGA consists of repeating units of glycolic and lactic acid, whereas PEAs are based on repeating units of glycolic acid and an amino acid. The two repeating units are arranged in an alternating fashion in the PEA, whereas PLGA represents a statistical copolymer.

Such PEAs, incorporating the hydrophobic amino acid valine, have been known since the pioneering works of Feijen and coworkers in the early 1990's [11]. Within the following decade, Feng et al. conducted intensive research on PEA featuring valine and isoleucine repeating units, also establishing synthetic routes toward block copolymers comprising poly(ethylene glycol) (PEG) [12]. Although the versatility of the incorporation of α-amino acid moieties within polyester materials has been explored, *e.g.*, for the attachment of targeting ligands, only a few reports exist regarding the use of hydrophobic PEA homopolymers for drug delivery purposes [9,13,14]. Instead, copolymers of lactide and/or glycolide with morpholine-2,5-diones have been studied [15–17]. To the best of our knowledge, only Lendlein and coworkers performed a direct comparison between oligo[(3-(S)-*sec*-butyl)morpholine-2,5-dione]diol and PLGA regarding dexamethasone encapsulation, despite the striking structural similarity of PEA made from morpholine-2,5-diones and PLGA [9].

In the present study, L-valine (Val) and L-isoleucine (Ile) based PEAs, as well as the respective block copolymers with a hydrophilic poly(2-ethyl-2-oxazoline) (PEtOx) block, were investigated. To date, PEG is the "gold standard" hydrophilic pharmapolymer [18]. PEG provides the nanoparticles with a "stealth effect", preventing their recognition by the immune system and prolonging their circulation time in the body [19]. However, PEGylated drug carriers and formulations containing PEG have been reviewed critically lately due to a recognized appearance of antibodies in humans originating from their intense use in, *e.g.*, salves, cremes, and as drug delivery components. This could limit their applicability in the near future. In consequence, PEtOxylated PEAs are expected to represent promising alternatives to PEG-PLGA, since PEtOx features a similar "stealth effect" as PEG [18,20].

In a previous study, Dirauf et al. synthesized various PEtOx-*b*-PEA block copolymers based on Val and Ile. The hydrophilic PEtOx polymer block was attached to various **PValG** and **PIleG** polymer blocks through the use of PEtOx macroinitiators [21]. The latter feature a degree of polymerization (DP) of 20 and, accordingly, a molar mass of 2000 g mol^{-1}, which is a frequently used molar mass for PEGs in biomedical applications [22].

The synthesized **PValG** and **PIleG** homopolymers and the PEtOx-*b*-PEA block copolymers are herein investigated with respect to their nanoparticle formation potential and stability. First, automated high-throughput (HT) nanoprecipitation in a 96-well-plate format was utilized for an initial screening based on small material quantities. In addition to nanoprecipitation of individual polymers, varying amounts of block copolymers were supplemented to the respective homopolymers in order to stepwise increase the hydrophilic portion in the formulation, enabling an investigation of the impact on the particle formation in terms of size, size distribution, and zeta potential.

Selected PEAs were used to encapsulate different lipophilic anti-inflammatory APIs, *i.e.* BRP-187 or BRP-201, in order to assess their potential as drug carrier materials and to evaluate whether differences between the two APIs can be identified due to their structural variations. Both water-insoluble compounds are representatives of the novel drug class of dual inhibitors that target the 5-lipoxygenase-activating protein (FLAP, required for leukotriene formation) and the microsomal prostaglandin E_2 synthase-1 (mPGES-1, required for PGE_2 formation). They are so-called lipid mediator class switch inducers (LMCSIs) and are of particular interest for pharmaceutical applications as they possess a superior pharmacological profile compared to established non-steroidal anti-inflammatory drugs (NSAIDs). This is due to the fact that they inhibit only the formation of pro-inflammatory PGE_2 and leukotrienes without affecting beneficial metabolites within the arachidonic acid cascade. In addition, they can accelerate the resolution of inflammatory processes through promotion of pro-resolving lipid mediators. Due to the strong plasma protein binding properties of BRP-187 and BRP-201,

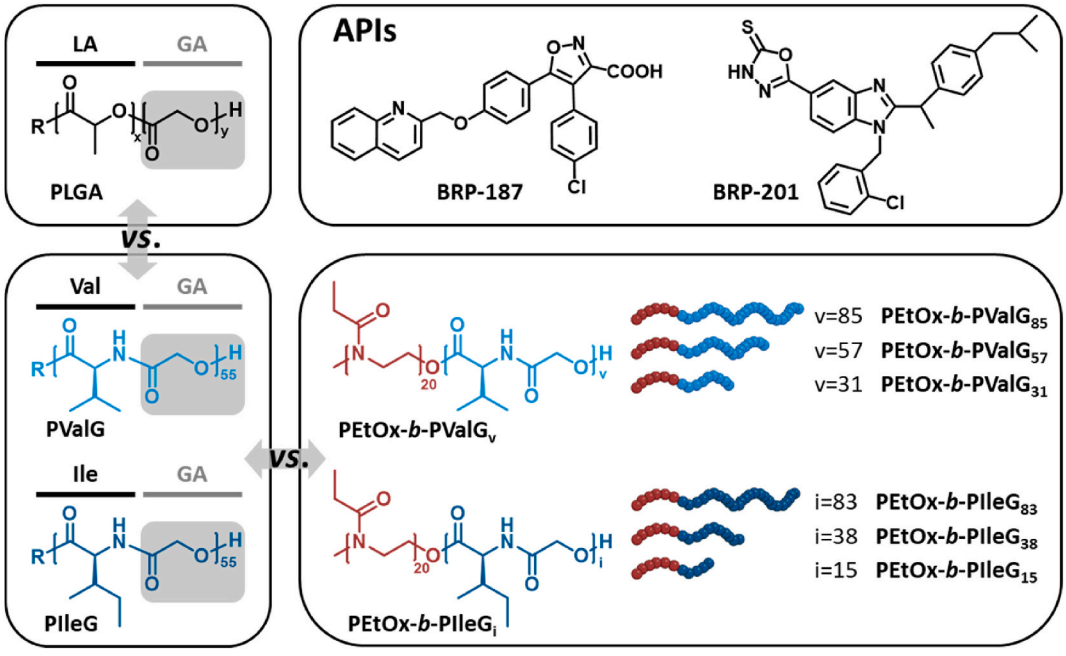

Fig. 1. Schematic representation of the used PEA homopolymers and PEtOx-*b*-PEA block copolymers in comparison to PLGA and the active pharmaceutical ingredients (APIs) used (LA = lactic acid, GA = glycolic acid).

they rely on the use of, *e.g.*, nanocarriers to achieve sufficiently high bioavailability also *in vivo* [23–25].

To this end, it was previously demonstrated that acetalated dextrans as well as PLGA, represent suitable carrier materials [6,26]. Nevertheless, the use of PLGA in drug formulation approaches may lead to the occurrence of free drug precipitates, and, thereby, an undesired increased interaction with plasma proteins [5]. Due to an expected additional hydrogen bonding of API and polymer, PEAs seem to offer the potential for improved, *i.e.*, more efficient encapsulation of the API and, thus, superior anti-inflammatory efficacy.

The possibility of hydrogen bonding between BRP-187 and BRP-201 with **PValG** and **PIleG** was investigated *via* atomistic molecular dynamics (MD) simulations. On this basis, the respective nanoparticles were prepared in larger batch sizes. PEtOxylated PEAs were used in addition to these two homopolymers to introduce a "stealth effect" (Fig. 1). Within the subsequent drug encapsulation studies, the following important nanoparticle properties were examined in respect to central aspects of the envisaged drug delivery applications: i) Nanoparticle formation and drug encapsulation, ii) stability and degradation of the nanoparticles in cell culture medium as well as in the presence of the enzyme proteinase K, iii) cellular uptake of the nanoparticles into HEK293 cells and into human macrophages (M1), their cytotoxicity as well as biocompatibility. Finally, the nanoparticles' ability to deliver the APIs BRP-187 and BRP-201 to inhibit FLAP-mediated leukotriene formation was examined. The results for the PEA homo- and block copolymer nanoparticles were compared with the PLGA nanoparticles formulated under the same batch conditions.

2. Materials and methods

2.1. Materials

The synthesis of the PEA homopolymers and PEtOx-*b*-PEA block copolymers is described elsewhere [21]. They were used without further treatment and key characterization data are provided in Table S1. BRP-187 and BRP-201 were synthesized based on established procedures [27]. Acetone (99+%, extra pure) was purchased from Acros Organics and ethyl acetate (ROTISOLV® ≥99.9 %, GC Ultra Grade) was received from Carl Roth GmbH. Resomer RG 502H (PLGA, M_w 7000 to 17,000 g mol^{-1}), poly(vinyl alcohol) (PVA) (Mowiol 4–88, M_w 31,000 g mol^{-1}), dimethylsulfoxide (DMSO, anhydrous ≥99.9 %) and all other materials were obtained from Sigma-Aldrich. Tetrahydrofuran (THF) was dried in a solvent purification system (SPS, Pure solv EN, InnovativeTechnology). Purified water from purification system (GenPure ultrapure water system, Thermo Scientific) was used in all stages of nanoparticle preparation, purification, and characterization studies. HPLC grade acetonitrile (CH_3CN) and water as well as formic acid (FA, ≥99.9 %) were purchased from VWR.

2.2. High-throughput formulation

For the high-throughput formulation (HT formulation), a liquid handling robot (CyBio FeliX, Analytik Jena GmbH) equipped with a choice head R 96/250 μL was utilized. The robot was programmed utilizing the CyBio Composer software. All liquid transfers were performed using disposable tips with a volume of 250 μL. At first, stock solutions of all polymers were prepared in THF with a polymer concentration of 2.5 mg mL^{-1}. Subsequently, with the assistance of a liquid handling robot, defined mixtures of homo- to copolymer solutions were prepared in a 96 well plate (Greiner Bio-One GmbH). The applied volumes are listed in Table S2. To produce nanoparticles, 25 μL of the mixed polymer solutions were injected into another 96 well plate that contained 200 μL of purified water per well to result in a solvent/non-solvent volume ratio during formulation of 0.125. The dispersions were mixed after injection by aspiration and release with a pipette tip five times. The plate was left on the bioshaker at 40 °C for 60 min to evaporate THF. The final amount of polymer per well was 0.0625 mg and the final nanoparticle concentration was 0.312 mg mL^{-1} in water. All formulations were prepared and analyzed in triplicate to evaluate the repeatability of the HT formulation procedure in general.

2.3. Automated high-throughput dynamic light scattering

For high-throughput dynamic light scattering (HT DLS) measurements, a 96 well plate was used (Greiner 96, poly-propylene 392 μL per well, flat bottom clear). For this purpose, 10 μL of the particle formulation were added to a prefilled plate that contained 100 μL of purified water with assistance of the robot. For the measurements, the plate was closed with a sealing tape (Sigma Aldrich). After equilibration of the dispersion, measurements on the HT DLS DynaPro Platereader III (Wyatt Technology Europe GmbH) were performed. The size distribution was calculated using the Software DYNAMICS® based on three acquisitions with 3 s per measurement and the following additional settings: Temperature 25 °C, dn/dc = 0.185 mL g^{-1}, RI (at 830 nm) 1.584, auto-attenuation on.

2.4. Nanoprecipitation in larger batches

For the preparation of the nanoparticles by nanoprecipitation in larger batches, a syringe pump (Aladdin AL1000-220) operating at a flow rate of 2 mL min^{-1} was used. The polymers (including PLGA) were first dissolved at a concentration of 5 mg mL^{-1} in THF. To obtain drug-containing nanoparticles, a 10 mg mL^{-1} API (either BRP-187 or BRP-201) stock solution in DMSO was added to the polymer solution to reach a ratio of API to polymer of 3 % (w/w). PVA was added to the aqueous phase at a concentration of 0.3 % (m/v), which was then used in a volume ratio of 10:1 with respect to the THF solution. The organic phase was injected into the aqueous phase at room temperature while stirring at 800 rpm and allowed to stir under a fume hood overnight. The next day, the nanoparticles were purified by centrifugation for 60 min at 20 °C at 11,000 rpm (5804 R centrifuge, Eppendorf). The supernatant was then removed and the nanoparticles were resuspended in water to achieve a theoretical concentration of 5 mg mL^{-1}. To this end, the dispersions were first vortexed, then placed in an ultrasonic bath for 30 min, and stored overnight in a refrigerator to allow equilibration of the particle dispersion. For further investigations, aliquots were freeze-dried (Lyophilizer Christ Alpha 2–4 LD plus). The mass of the nanoparticles was determined by using a MYA 11.4Y microbalance (Radwag Waagen) and the final concentration was calculated by dividing the mass of the lyophilizate by the volume used for lyophilization.

2.5. Dynamic and electrophoretic light scattering

Dynamic light scattering (DLS) and electrophoretic light scattering (ELS) were applied to determine the size and zeta potentials (ζ) of the nanoparticles, respectively. For that purpose, a Zetasizer Nano ZS or Zetasizer Ultra (Malvern Panalytical GmbH) was utilized. The Zetasizers operate with a laser wavelength of 633 nm. DLS was measured in polystyrene microcuvettes (Brand GmbH + Co KG) at 25 °C and a back-scattering angle of 174.7°. The intensity-weighed hydrodynamic diameter (d_H) and corresponding polydispersity index (PDI) of the nanoparticles are reported. Furthermore, DTS1070 capillary cuvettes (Malvern Panalytical GmbH) were used for ELS investigations. The selected samples of the HT-formulations (200 μL) were further diluted with 800 μL of pure water and measured in a DTS1070 capillary cuvette three times for 10 s at 25 °C for size analysis *via* DLS as well as in automatic mode for the determination of the zeta potential by ELS. For the batch formulations, 10 μL of the particle suspension was diluted with 1 mL of deionized water and measured five times (15 runs each with a run time of 1.68 s) for DLS and three times in ELS.

2.6. Stability investigation via DLS

The stability of the unloaded nanoparticles formulated *via* batch nanoprecipitation (**PValG**, **PIleG, PEtOx-*b*-PValG$_{85}$, PEtOx-*b*-PIleG$_{83}$** and PLGA) was monitored by DLS. For this purpose, the nanoparticles were diluted with cell culture medium (D10, low glucose Dulbecco's modified eagle's medium (DMEM)) at a volume ratio of 1:1 and incubated at 20 °C as well as at 37 °C. The nanoparticles' size and size distribution were measured up to 120 h with a fixed attenuator of 7. In order to also provide long-term data on the stability of the nanoparticles at body temperature, the particle suspensions were stored in an incubator at 37 °C in between measuring intervals.

2.7. Degradation studies with proteinase K

The degradation behavior of the four PEA nanoparticles obtained from batch nanoprecipitation and the PLGA control sample was investigated by DLS measurements. For this purpose, the nanoparticles in suspension (initial concentration 2 mg mL^{-1}) were incubated with a proteinase K solution (in water) at 37 °C in mass ratios from 1:3 to 1:238 (particle:proteinase K). The mean count rate was used as a readout (at a fixed attenuator of 7) and the initially measured count rate was set equal to 100 %; the count rate development over time is represented in percentages.

2.8. Scanning electron microscopy (SEM)

A Sigma VP field emission scanning electron microscope (Carl-Zeiss AG, Germany) was used to image the nanoparticles. Micrographs were acquired with the InLens detector at an acceleration voltage of 3 kV and 6 kV, respectively. Nanoparticle formulations were initially diluted with water in a 1:5 ratio. 10 μL was pipetted onto mica substrates and air dried. Prior to the measurements, the samples were coated with a thin layer of platinum (4 nm) using sputter coating (CCU-010 HV, Safematic).

2.9. Hemolysis assay and erythrocyte aggregation

The assays were performed according to a previously published protocol [28]. All animal husbandry is performed in compliance with the relevant European and German laws, institutional guidelines and to state including the institutional animal committee. The sheep blood was taken from general veterinary management of the animal health (Institut für Versuchstierkunde und Tierschutz/Laboratory of Animal Science and Animal Welfare, Friedrich Schiller University Jena). To assess the hemolytic activity of the nanoparticle suspensions, blood from sheep was collected in heparinized-tubes, centrifuged at 4500×*g* for 5 min, and the pellet was washed three times with cold phosphate buffered saline (PBS, pH 7.4; biowest). Afterward the pellet was resuspended in PBS pH 7.4 in a ratio of 1:10 (v/v). The erythrocyte suspension was mixed with the nanoparticle suspension in a ratio of 1:1 (v/v) and incubated at 37 °C and 5 % CO_2 for 1 h. Samples were tested at three different concentrations: 10, 50 and 100 μg mL^{-1}. After centrifugation at 2400×*g* for 5 min the hemoglobin release into the supernatant was determined spectrophotometrically using a microplate reader (TECAN Infinite M200 PRO) at λ = 544 nm with a reference wavelength at λ = 630 nm. Complete hemolysis (100 %) was achieved using 1 % Triton X-100 (Sigma-Aldrich) serving as positive control. PBS served as negative control. A value of less than 2 % hemolysis rate was taken as nonhemolytic.

For the examination of the erythrocyte aggregation, erythrocytes were isolated and mixed with the nanoparticle suspensions as described above. Incubation was done in a clear flat bottomed 96-well plate at 37 °C for 2 h. The absorbance was measured at λ = 645 nm in a microplate reader (TECAN Infinite M200 Pro). 10 kDa branched poly (ethylene imine) (PEI) at a concentration of 50 μg mL^{-1} (Polyscience) was used as positive control while PBS treated cells served as the negative control. Absorbance values of the test solutions lower than the negative control were regarded as aggregation.

Hemolysis assay and erythrocyte aggregation assay were performed with blood from three different donors and were run in triplicates.

2.10. UV–Vis spectroscopy

The loading capacity (LC) of the nanoparticles with BRP-187 and BRP-201 was determined using a UV–Vis plate reader (Infinite M200 Pro plate reader, Tecan Group Ltd.) according to a protocol published previously [5]. For this, the freeze-dried samples were dissolved in the same volume of UV-grade DMSO that was previously freeze-dried as an aliquot (see **2.4**). The UV absorbance of 100 μL of the dissolved nanoparticles was measured undiluted and diluted (1:2, 1:4, and up to 1:8 (v/v), if necessary) at λ = 316 nm with 3 × 3 multiple reads per well and a 2000 μm wide well margin using a Quartz 96-well plate (Hellma). The concentration of BRP-187 and BRP-201 in the nanoparticles was determined from a calibration curve of APIs. For this purpose, a new calibration curve was determined for each replicate in the concentration range of 1.95–250 μg mL^{-1} in DMSO. The LC values were calculated using the following formula:

$$LC = \frac{mass\ of\ drug\ recovered}{mass\ of\ particle\ recovered}\ x\ 100$$

The residual amount of PVA (%, w/w) in the freeze-dried nanoparticles was also quantified by UV–Vis spectroscopy enabled by formation of a PVA-iodine complex according to a previously published protocol [29]. The fluorescence measurements of the nanoparticles (c = 1 to 3 mg mL^{-1}) containing the fluorescently labeled BRP-187 (fluo-BRP-187) for cellular uptake experiments were measured at λ_{ex} = 510 nm and λ_{em} = 650 nm with a gain of 100–150 using a Quartz 96-well plate (Hellma).

2.11. High performance liquid chromatography (HPLC)

The fluo-BRP-187 content in the formulations was determined by HPLC. For that purpose, an UltiMate 3000 Dionex UHPLC chromatographic system from Thermo Fisher Scientific equipped with a binary pump and a diode array detector (DAD) was used. Elutions were monitored at 290 nm, being the absorbance maximum of the drug. The autosampler temperature was set to 20 °C and the column oven temperature was set to 40 °C. The injection volume was 10 μL and a flow rate of 1.5 mL min^{-1} was utilized. For addressing drug analysis, a Chromolith® High Resolution RP-18 endcapped monolithic column (100 × 4.6 mm) from Merck KGaA was used as the stationary phase [30]. The mobile phase consisted of CH_3CN and 0.1 % FA in water (v/v). The starting elution conditions were kept constant at 5/95 CH_3CN/aqueous FA (%, v/v) for 1.5 min. After that a linear mobile phase gradient was programmed to 100 % CH_3CN within 8.5 min, followed by a 3-min isocratic hold. Afterward, the initial elution conditions, *i.e.*, 5 % CH_3CN were re-established within 1 min and the column was equilibrated for 2.5 min before the next injection. Further details on sample preparation procedures and calibration for drug quantification can be found in Section 12 of the SI. For data evaluation, the Thermo Scientific™ Dionex™ Chromeleon™ 7 Chromatography Data System was used.

2.12. Molecular dynamics simulations

Molecular dynamics (MD) simulations were performed to analyze the miscibility between PEA polymers and drugs analogous to a previously published study [7]. According to the Flory-Huggins miscibility theory, the change of Gibbs free energy of mixing is defined as [31,32].

$$\Delta G_{mix} = RT\left(\frac{x_p}{r_p}\varphi_p + \frac{x_d}{r_d}\varphi_d + x_p x_d \chi\right) \quad (1)$$

where R is the gas constant, T is the temperature, x_i, r_i, and φ_i are the mole fraction, degree of polymerization, and volume fraction, respectively, of a polymer (i = p) and a drug molecule (i = d, $r_d = 1$). χ is the Flory-Huggins (FH) interaction parameter. The FH parameter can be calculated using two methods, denoted here as methods I and II [33,34]. Method I is the simplest one and expresses the FH parameter in terms of Hildebrand solubility parameters δ_i of pure components

$$\chi_I = \frac{V_m}{RT}(\delta_p - \delta_d)^2 \quad (2)$$

where V_m is the molar volume of one lattice segment. δ_i is defined as the square root of the cohesive energy density (CED), which can be obtained from MD simulations of pure compounds. The more accurate method II employs atomistic MD simulations of actual binary mixtures with χ_{II} defined as

$$\chi_{II} = \frac{V_m}{RT}\left(\varphi_p CED_p + \varphi_d CED_d - CED_{p-d}\right) \quad (3)$$

where φ_p and φ_d are the volume fractions of a polymer and a drug, respectively. CED_p and CED_d are the corresponding cohesive energy densities of a polymer and a drug, respectively, and CED_{p-d} is the cohesive energy density of a polymer-drug mixture (**SI Section 9**).

2.13. Uptake studies of nanoparticles by live-cell confocal imaging

The uptake of PEA nanoparticles by HEK293 (WT) cells was studied for a timescale of 5 h *via* live-cell confocal imaging, as it provides the capability of optical sectioning. HEK293 (WT) cells were cultured at 37 °C and 8.5 % CO_2. Experiments were performed in glass-bottomed 35 mm culture dishes (IBIDI) using DMEM (high-glucose) supplemented with 10 % fetal bovine serum (FBS), 1 % Penicillin/Streptomycin and 2 mM L-Glutamine. For live cell imaging, DMEM was exchanged for phenol red free Leibovitz 15 (L-15). An approximate number of 2×10^5 cells per dish was allowed to grow and attach to the surface for 24 h until a confluence of around 60 % was reached. For particle incubation, the DMEM medium was replaced by 0.5 mL of L-15 and brought to the microscope incubator (37 °C, 5 % CO_2) where 0.5 mL of the nanoparticles diluted in L-15 was added to the dish. The final concentration of the fluo-BRP-187 was 3 μM. Immediately after adding the nanoparticles, cells were imaged using an inverted confocal microscope (Zeiss CLSM 980) with a 20× air objective NA 0.80. Samples were excited using a 488 nm laser (1 % intensity) and the emission was collected by a GaAsP-Photomultiplier-Tube (PMT) in the spectral interval of 501 to 696 nm. The transmitted intensity was recorded in an extra channel using a Multialkali T-PMT. For each sample, an area containing a sufficient number of cells was selected, and a region of interest (ROI) of approximately 400 × 400 μm was imaged every 3 min at a pixel size of 149 nm. To correct for focus drifting in the axial direction, the DefiniteFocus3 module was used to keep a constant distance between the microscope objective and the samples' glass bottom.

For the phagocytic uptake studies into M1 macrophages, cells were seeded on a multi-well glass-bottom slide (IBIDI) coated with poly-L-lysine to promote cell adhesion. The nanoparticles were incubated with the cells at a concentration of 0.2 mg mL^{-1}. Immediately after particle application, a 16-particle area of approximately 750 × 750 μm was selected and imaged (CLSM 980 Zeiss). Images were acquired every 43 min over a period of 14 h with a pixel size of 99 nm. The sample drift was corrected *via* the DefiniteFocus3 module. Fluorescence was excited using a 488 nm laser (0.2 % intensity) and collected in the spectral interval of 554 nm to 696 nm in a GaAsP-PMT using a 40 × NA 1.2 water objective. The transmitted light intensity was collected in an extra channel by a Multialkali-PMT.

2.14. Cytotoxicity assays in human neutrophils

Cytotoxicity was studied by analysis of lactate dehydrogenase (LDH) release (cell integrity) in human neutrophils according to a previously published protocol [35]. The release of LDH from the cells was analyzed using the CytoTox 96® Non-Radioactive Cytotoxicity Assay (Promega GmbH). In brief, 10^6 neutrophils per vial were suspended in PBS containing 0.1 % glucose plus 1 mM $CaCl_2$. Neutrophils were incubated with differential nanoparticles and lysis control with 0.2 % Triton X for 1 h at 37 °C. Supernatant was transferred to Eppendorf tubes and centrifuged (400×*g*, 4 min, RT). 50 μL of supernatant from each cup was transferred in a 96-well plate. Afterward, 50 μL of substrate mixture was added and incubated for 30 min at RT in the dark. 50 μL of stop solution (1 M acetic acid) was added. The photometric measurement was performed at 490 nm using a Multiskan Spectrum plate reader (Thermo Fisher Scientific).

2.15. Analysis of FLAP-dependent 5-LOX product formation in human neutrophils

For isolation of neutrophils, leukocyte concentrates were prepared from peripheral blood obtained from healthy adult male and female donors that received no anti-inflammatory treatment for the last 10 days (Institute of Transfusion Medicine, Jena University Hospital) according to a previously published protocol [6]. The approval for the protocol was given by the ethical committee of the Jena University Hospital and all methods were performed in accordance with the relevant guidelines and regulations. The leukocyte concentrates were mixed with dextran (from leuconostoc spp. MW ~40,000, Sigma Aldrich) for sedimentation of erythrocytes and the supernatant was centrifuged on lymphocyte separation medium (Histopaque®-1077, Sigma Aldrich). Contaminating erythrocytes in the pelleted neutrophils were removed by hypotonic lysis (using water). Neutrophils were subsequently washed twice in ice-cold phosphate-buffered saline (PBS) pH 7.4 and finally resuspended in PBS pH 7.4. For evaluation of the effects of the API on 5-LOX product formation in neutrophils, cells (5×10^6 mL^{-1}) were pre-incubated with free API and API encapsulated into nanoparticles for 1 h at 37 °C. The cells were then stimulated with 2.5 μM Ca^{2+}-ionophore A23187 (Cayman) for 10 min, and the incubation was stopped with 1 mL ice-cold methanol containing 200 ng mL^{-1} prostaglandin B1 (PGB_1) as internal standard. Samples were subjected to solid phase extraction and formed 5-LOX products (LTB_4, *trans*-isomers of LTB_4, 5-hydroperoxyeicosatetraenoic acid (5-HETE)) were separated and analyzed by RP-HPLC as described previously [36].

2.16. Analysis of leukotriene and prostaglandin formation in human blood

The analysis of leukotriene and prostaglandin formation in human blood was performed analogously to a previously published protocol [6]. Freshly withdrawn whole blood in Li-heparin Monovettes (Sarstedt) from healthy adult donors that had not received any anti-inflammatory treatment the last 10 days was provided by the Institute of Transfusion Medicine, Jena University Hospital. The blood was pre-incubated with free API and API encapsulated into nanoparticles for 5 h and subsequently stimulated with 3 % *S. aureus*-conditioned medium for 90 min. The reaction was stopped with ice-cold methanol containing the deuterium-labeled internal standards d8-5 S-HETE, d4-LTB_4, d5-LXA_4, d5-RvD2, and d4-PGE_2 (500 pg, each). Samples were kept at −20 °C for one day to allow protein precipitation. After centrifugation (2000×*g*, 4 °C, 10 min) 8 mL acidified water (PBS–HCl) was added (final pH = 3.5) and samples were subjected to solid phase extraction using RP-18 columns. The lipid mediators LTB_4 and PGE_2 were analyzed by ultra-performance liquid chromatography-tandem mass spectrometry (UPLC-MS-MS) using an Acquity UPLC system (Waters) and a QTrap 5500 Mass Spectrometer (Sciex) equipped with an electrospray ionization source as reported before [37].

3. Results and discussion

In the previous study from Dirauf et al., initial formulation of the PEA homopolymers and PEtOx-*b*-PEA block copolymers indicated their potential for the creation of nanosized nanoparticles or vesicles [21]. The latter were observed in particular for block copolymers containing a low fraction of PEA. In order to form nanoparticles, a sufficient hydrophobicity of the polymers achieved by the polymer composition is required.

More detailed formulation studies including the use of block copolymers in coformulations with homopolymers, in order to increase the hydrophobicity of the nanoparticles, are presented here. The overall stability as well as the suitability of PEAs as drug carrier materials are described in the following.

3.1. Automated high-throughput (HT) co-formulations of PEA polymers

Aiming at an initial assessment of the particle formulations containing **PValG**, **PIleG** and their respective block copolymers **PEtOx-*b*-PValG$_v$** and **PEtOx-*b*-PIleG$_i$** (Fig. 1 and Table S1), automated nanoparticle formulation in a 96-well-plate format was performed *via* HT nanoprecipitation by utilization of a liquid handling robot (Table S2) [38]. Besides the individual polymers, also mixtures of homo- and block copolymers were formulated to gain deeper insights into the particle formation, which is often influenced by the ratio of hydrophobic and hydrophilic segments within the carrier material [39,40]. Since the size of the nanoparticles is also known to affect their accumulation in specific body compartments, the impact of the starting material on the particle size also needed to be investigated. In addition to the automated formulation approach, the nanoparticles were studied using a HT DLS to determine the particle size and the PDI for each formulation. The mean z-average values (herein referred to as mean hydrodynamic diameter (d_H)), and the respective mean PDI values are presented in Fig. 2 and Tables S3 and S4.

Mean hydrodynamic diameters of d_H = 175 nm (PDI = 0.18) and d_H of 162 nm (PDI = 0.16) were obtained for the **PValG** nanoparticles as well as for the **PIleG** nanoparticles, respectively. With the stepwise addition of the respective copolymers **PEtOx-*b*-PValG$_v$** and **PEtOx-*b*-PIleG$_i$**, the mean sizes decreased for most of the formulations (Fig. 2, Tables S3 and S4). The smallest particle sizes, in the range of 100 nm, were obtained for the copolymers with the shortest hydrophobic PEA block, *i.e.*, **PEtOx-*b*-PValG$_{31}$** and **PEtOx-*b*-PIleG$_{15}$**. With the exception of the formulations containing 90 % and 100 % **PEtOx-*b*-PValG$_{31}$** or **PEtOx-*b*-PIleG$_{15}$**, all PDI values were rather low (0.13 < PDI <0.22, Fig. 2, Table S3 and Table S4), which indicates that almost all individual polymers and also the polymeric mixtures formed nanoparticles in the size range of 96–191 nm. In addition, the variations of the nanoparticle sizes were calculated according to Gaussian statistics and are presented in Figs. S3 and S4 [41].

Since the surface charge of the nanoparticles represents another important property that influences the interaction of the nanoparticles with the cells, ELS measurements were performed [42]. The zeta potential values from all formulations of the **PValG** and **PIleG** polymers with the PEtOxylated block copolymers are presented in Table S5 in dependence of the mass ratio (in wt%) used for the formulation. All nanoparticle formulations revealed a negative zeta potential, which is decreasing with increasing content of the PEtOx block copolymers (Fig. S5).

Overall, the experiments clearly indicated that the PEA homo- and block copolymers can be formulated into nanoparticles under the selected conditions and that specific co-formulations can be used to selectively influence certain particle properties, such as size, hydrophilicity, and surface charge. The experiments demonstrated furthermore that the PEA particle formulation can easily be performed in a 96-well plate format for a quick and straightforward structure-property screening. The low standard deviation (SD) values of the mean sizes for the three individually prepared formulations demonstrates the repeatability and reliability of the HT formulation, utilizing only small amounts of the respective polymers (Fig. 2).

3.2. Transfer to larger batch size

In order to enable further investigations of the PEA nanoparticles, larger quantities of the dispersions were required. Hence, the formulation procedure was transferred to larger batch format and performed with an increased initial polymer concentration of 5 mg mL^{-1} as well as with the surfactant poly(vinyl alcohol) (PVA), which is required as stabilizer for the following drug encapsulation experiments. Since BRP-187 and BRP-201 are rather hydrophobic APIs, the homopolymers **PValG** and **PIleG** as well as the two block copolymers **PEtOx-*b*-PValG$_{85}$** and **PEtOx-*b*-PIleG$_{83}$** were selected for additional studies. These four systems feature the highest hydrophobic character, which is expected to be beneficial for the encapsulation of the lipophilic APIs. Additionally, PLGA was used for nanoparticle formulation under the same conditions for comparison. Initially, unloaded nanoparticles were prepared in

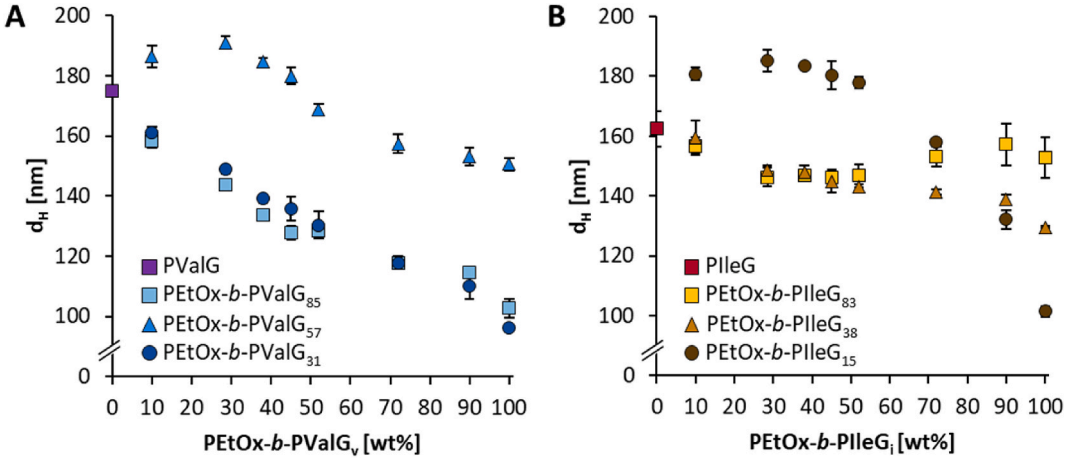

Fig. 2. Z-average hydrodynamic size values (d_H) obtained by dynamic light scattering from the co-formulation of (**A**) **PValG** and (**B**) **PIleG** homopolymers with the PEtOxylated block copolymers **PEtOx-*b*-PValG$_v$** (v = 85, 57, 31) and **PEtOx-*b*-PIleG$_i$** (i = 83, 38, 15) in dependence of the mass ratio (in wt%) used for the formulation. The respective mass ratio (in wt%) of the homopolymer in the co-formulation is calculated as **PValG** = 100 wt% - **PEtOx-*b*-PValG$_v$** wt% and **PIleG** = 100 wt% - **PEtOx-*b*-PIleG$_i$** wt%. The nanoparticles were formulated *via* HT-nanoprecipitation in a 96 well plate format using polymer solution concentrations of 2.5 mg mL^{-1} in THF. Results are means of n = 3 individual formulations and the SD refers to the deviations for all formulations. All PDI values ranged from 0.13 to 0.22, with the exception of the formulations containing 90 % and 100 % **PEtOx-*b*-PValG$_{31}$** (PDI = 0.28 each) and **PEtOx-*b*-PIleG$_{15}$** (PDI = 0.31 and 0.44).

larger batches *via* nanoprecipitation. Nanoparticles with mean sizes similar to that of the HT-formulations were obtained, demonstrating the feasibility of the HT approach for initial screenings at low scale (Table S6). However, zeta potential measurements revealed decreased surface charges for the larger batches, which might be due to the presence of the surfactant PVA in the dispersions [43] (Fig. 3).

3.2.1. Biocompatibility, stability, and biodegradability

In addition to the general physicochemical properties of the nanoparticles such as size, PDI, and zeta potential, the biocompatibility, stability, and biodegradability of the PEA nanoparticles were investigated to prove their suitability for *in vitro* and *in vivo* applications. On the one hand, the nanoparticles must be biocompatible and harmless as well as able to sufficiently protect the API when used as a drug delivery vehicle. On the other hand, the carrier must be able to release the API and be degradable to enable its elimination from the body. The biocompatibility of the nanoparticles was tested *via* a red blood cell aggregation test and a hemolysis assay at particle concentrations of 10, 50, and 100 μg mL^{-1}. None of the particle systems revealed hemolytic effects or caused red blood cell aggregation (Fig. S7A and B). Cytotoxicity was tested *via* LDH-assay in neutrophils, revealing no cytotoxic effect (Fig. S7C).

To investigate their stability, the nanoparticles were incubated up to 120 h at a temperature of 20 °C and 37 °C in culture medium and the size as well as PDI were monitored by DLS [26]. No change of particle size and size distribution was observed, indicating the presence of stable particle dispersions without any degradation or undesirable aggregation. Similar to the PLGA control, all PEA nanoparticles revealed appreciable stability in culture medium at both temperatures within the measured timeframe (Fig. S8).

Subsequently, the biodegradability of the PEA-based nanoparticles was investigated in order to gain information on the release behavior of the water-insoluble APIs. The degradation of the particles depends on the particle properties, for instance with regard to their size and the

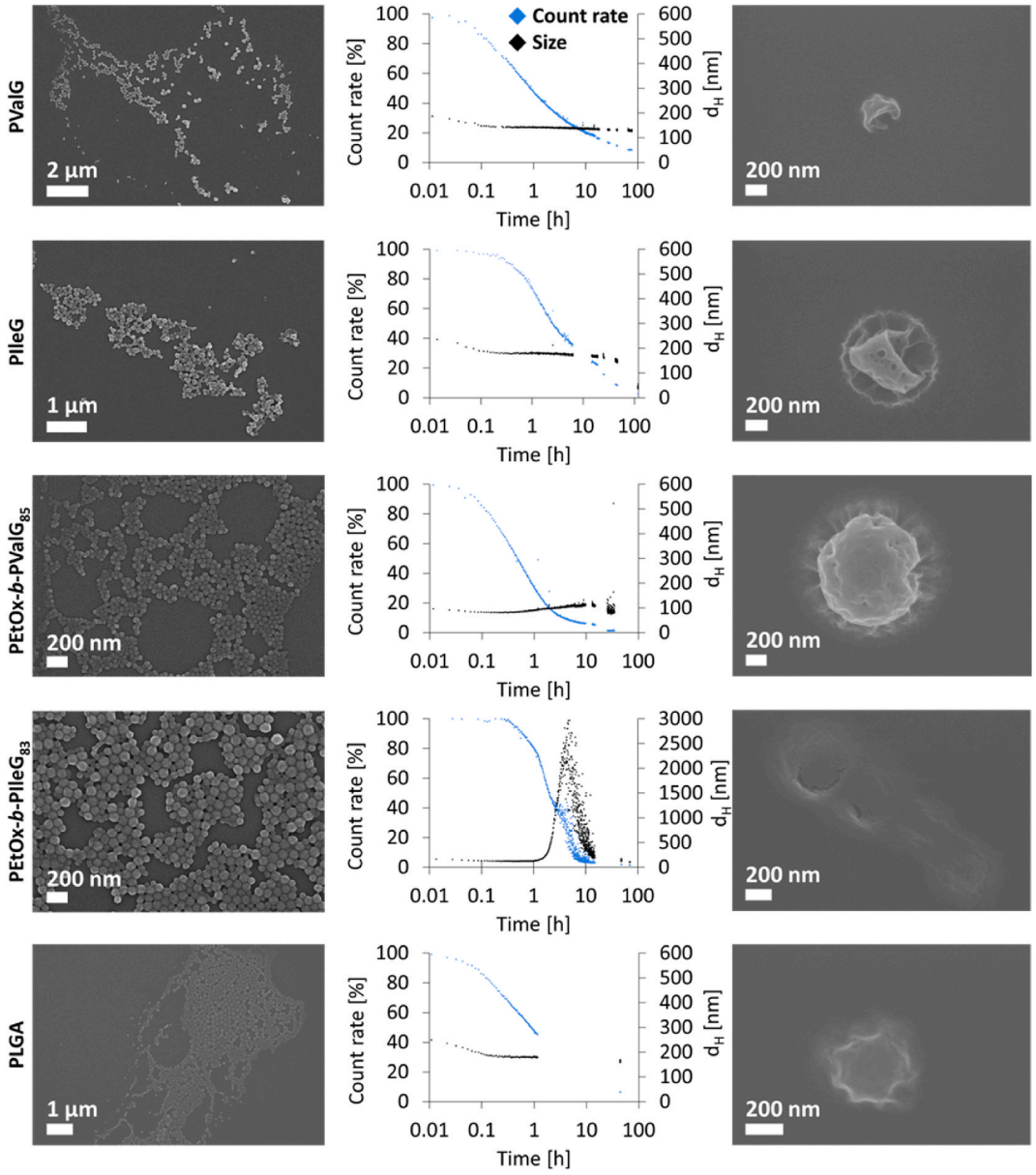

Fig. 3. Particle degradation at 37 °C over time. Nanoparticles were resuspended in water and enzyme proteinase K with the mass ratio of nanoparticle to enzyme being 1:23 (**PValG**, t_{50} = 0.87–0.90 h), 1:238 (**PIleG**, t_{50} = 2.52–2.58 h), 1:3 (**PEtOx-*b*-PValG$_{85}$**, t_{50} = 0.47–0.49 h), 1:23.5 (**PEtOx-*b*-PIleG$_{83}$**, t_{50} = 1.99–2.03 h), and 1:20 (PLGA, t_{50} = 0.89–0.90 h). Scanning electron microscopy images of a sample residual 24 h after addition of the proteinase K solution.

associated differences in the ratio of volume to surface area, but also essentially on the properties of the polymers as starting material. The degradation of these polymers can occur, for instance, through enzymatic degradation *via* proteases or esterases, such as lipases [44,45]. Proteinase K solution was used herein due to its broad specificity [46]. In preliminary studies (data not shown) various ratios of nanoparticles to proteinase K were tested to estimate the amount that would lead to almost complete degradation of the nanoparticles in a reasonable time frame. The t_{50} value refers to the point in time at which half of the initial count rate in DLS recordings is reached (Fig. 3).

The resulting mass ratios of nanoparticles to enzyme solution ranged from 1:3 to 1:238 (Fig. 3). **PLGA** and **PValG** nanoparticles revealed a similar continuous degradation profile at similar polymer to enzyme ratios, showing that the exchange of the lactic acid repeating unit by valine (Fig. 1) does not affect the degradation behavior in a significant manner. The **PIleG** nanoparticles degraded considerably slower, even at markedly higher proteinase K amounts. The decelerated degradation may be due to the increased hydrophobicity of the isoleucine unit induced by the *sec*-butyl substituent, which also increases the sterical demand, thereby hindering the accessibility for the enzyme. Bulk **PValG** is an amorphous polymer featuring a T_g value of 71 °C. **PIleG** is semi-crystalline (T_m = 95 °C, degree of crystallinity 35 %) [21]. An increased stability or accessibility of crystalline domains might also contribute to the slower degradation kinetics of the **PIleG** nanoparticles, although the degree of crystallinity in nanoparticles formed from **PIleG** might differ from that of the bulk material.

An accelerated degradation for the PEtOx-block copolymers was observed even at low enzyme concentrations, irrespective of the type of PEA. This might be due to the smaller size of the nanoparticles since a smaller particle size increases the contact surface per volume particle available for the enzyme. In addition, the degree of polymerization of the block copolymer segments suggests the presence of PEtOx segments in the particle core. This would increase its hydrophilicity, while decreasing its density, which would make the particle more susceptible to degradation. Furthermore, the **PEtOx-*b*-PIleG$_{83}$** nanoparticles apparently degraded in a different manner compared to all other nanoparticles (**Fig. 3**). Aggregates were formed at some point during the degradation, as indicated by the increase of the mean size at overall decreasing count rates. However, these aggregates seem to degrade subsequently as they decreased in size, and the count rate decreased over time.

Overall, all nanoparticles were biodegradable, as also demonstrated by SEM measurements. Whereas the SEM measurements revealed the presence of uniform, spherical nanoparticles prior to degradation, only a few residuals of nanoparticles with significantly altered morphology could be found after incubation with proteinase K (Fig. 3).

3.3. Drug-loaded PEA nanoparticles

The unloaded PEA nanoparticles based on **PValG**, **PIleG, PEtOx-*b*-PValG$_{85}$** and **PEtOx-*b*-PIleG$_{83}$** prepared by batch nanoprecipitation fulfilled all main prerequisites as carriers for drug delivery applications, *i.e.*, safety, stability, and biodegradability. Hence, these polymers were used for the encapsulation of the hydrophobic and anti-inflammatory APIs BRP-187 and BRP-201 (Fig. 1) [24,25].

Table 1
Flory-Huggins (FH) parameters χ_I and χ_{II} calculated with the method I and II, respectively, the corresponding free energy of mixing (J/mol) and solubility limits (wt%) for the simulated mixtures of **PValG** and **PIleG** with BRP-187 and BRP-201.

Polymer	API	API weight ratio [wt%]	χ_I	χ_{II}	ΔG_{mix} (χ_I) [J mol^{-1}]	Solubility limit (χ_I) [wt%]	ΔG_{mix} (χ_{II}) [J mol^{-1}]	Solubility limit (χ_{II}) [wt%]
PValG	BRP-187	1	0.73	2.63	−39.1	5.0	−26.7	1.5
PValG	BRP-201	1.1	0.13	3.85	−49.6	20.2	−16.1	1.5
PIleG	BRP-187	1	1.31	2.68	−39.1	3.5	−26.7	1.4
PIleG	BRP-201	1	0.39	3.23	−47.3	8.7	−21.8	1.6

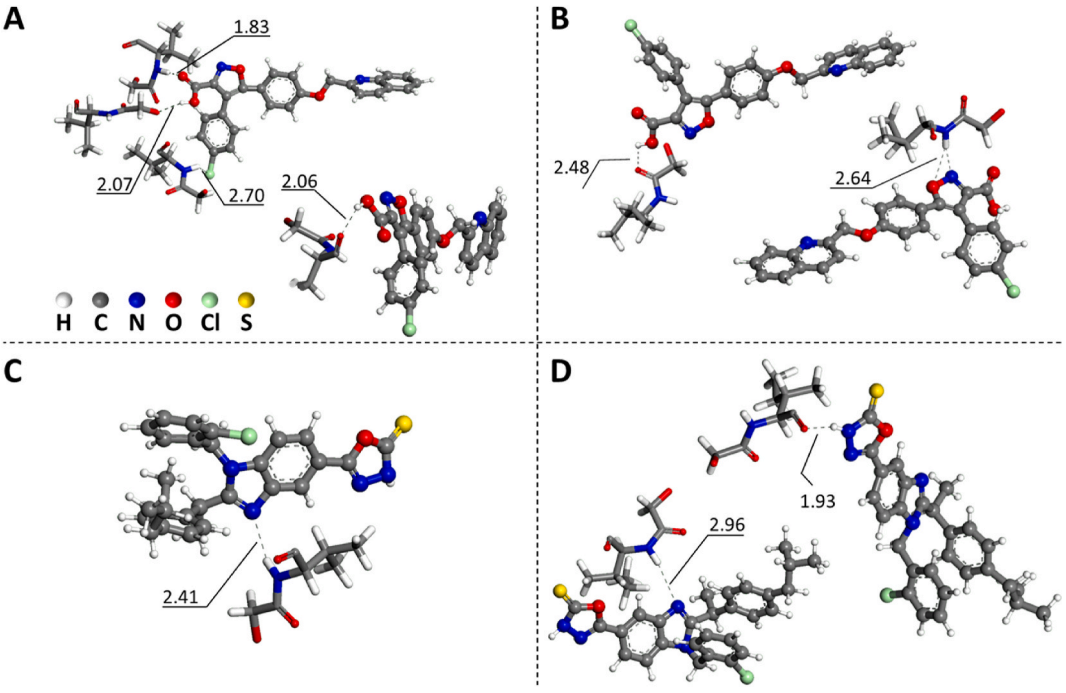

Fig. 4. Ball-and-stick representation of polymer segment – API interactions. (**A**) **PValG** with BRP-187, (**B**) **PIleG** with BRP-187, (**C**) **PValG** with BRP-201, and (**D**) **PIleG** with BRP-201.

3.3.1. Polymer-API interactions

An efficient encapsulation requires a favorable interaction of the API with the carrier material. The Gibbs molar energy of mixing is a parameter that can provide information about API-carrier material interaction [7]. It was therefore calculated for the mixtures of **PValG** and **PIleG** with BRP-187 and BRP-201 using the FH theory. The method was previously validated by comparison with experimentally determined thermodynamic parameters [7].

Table 1 shows the calculated Gibbs free energy of mixing (ΔG_{mix}). It is negative for the four simulated mixtures incorporating roughly 1 wt% of API, using both, the simpler method I based on Hildebrand solubility parameters (χ_I values) and the more accurate method II based on CED (χ_{II} values). Thus, the polymers are considered to be miscible with the API at a mass fraction that is commonly applied for the formulation of API into nanoparticles. However, the values of the FH parameters (χ) above 0.5 indicate that the range of miscibility between the drug and the polymers is generally limited. Using equation (1), we estimated the miscibility limit of PEA polymers with BRP-187 and BRP-201. As shown in Table 1, the less accurate method I predicts the miscibility limit to be between 3.5 and 20.2 wt%. However, the more accurate calculations using method II consistently predict a miscibility limit of about 1.5 wt%.

The interaction between API and polymer is shown for each system in Fig. 4, Figs. S9a and b. Indeed, hydrogen bonding contributes to the miscibility. As both API feature hydrogen bond donors (the carboxylic acid functionality in BRP-187 and one nitrogen atom in the oxadiazole-based heterocycle in BRP-201), interactions with ester and amide oxygen atoms of the PEA were seen. In addition, the amide moieties of the PEA act as hydrogen bond donors as they are in close proximity to various hydrogen bond acceptors of the API (*e.g.*, the isoxazole ring and chlorine atom of BRP-187, or the imidazole ring of BRP-201).

Based on the *in-silico* studies, both homopolymers are theoretically suitable for the encapsulation of the two APIs. As the hydrophilic PEtOx blocks will tend to arrange themselves preferably towards the particle surface, it can be assumed that the PEA blocks mainly form the hydrophobic core of the nanoparticles where the active ingredient molecules are incorporated. However, the presence of a few PEtOx segments within the particle core is likely due to the degrees of polymerization of the individual blocks in the PEtOx block copolymers. As this might influence the interaction with the API, the *in-silico* data are hence to be treated with prudence in respect to encapsulation of API into block copolymers.

3.3.2. Encapsulation of BRP-187 and BRP-201

To evaluate the encapsulation ability of the polymer systems with API, the homopolymers **PValG** and **PIleG** as well as the block copolymers **PEtOx-*b*-PValG$_{85}$** and **PEtOx-*b*-PIleG$_{83}$** were formulated *via* nanoprecipitation with BRP-187 and BRP-201, respectively. A drug feed of 3 wt% with respect to the polymer was applied in the preparations. The purified formulations were characterized with respect to their size, size distribution, zeta potential, and their loading capacity (LC) for the drug (Fig. 5 and Fig. 6, Tables S10a and S10c).

All LC values ranged from 0.5 wt% to 1.5 wt% referred to total particle mass, as determined by absorbance measurements. The encapsulated amounts of API within the nanoparticles are in accordance with the MD simulations, which suggested miscibility of the API and polymer for 1.5 wt% drug. Upon the introduction of an API, the particle sizes increased, in particular, when BRP-201 was used. BRP-201 was also encapsulated to a greater extent than BRP-187, with the exception of the nanoparticles prepared from **PEtOx-*b*-PValG$_{85}$**. According to the DLS data, the valine-based polymers produced smaller nanoparticles than polymers comprising isoleucine, which is only significant for the BRP-201 loaded nanoparticles. The introduction of the PEtOx blocks decreased the size of all API-loaded nanoparticles significantly (Table S6b, Tables S10b and S10d). All PDI values were below 0.1, which represents a monomodal size distribution (Fig. 5, Tables S10a and

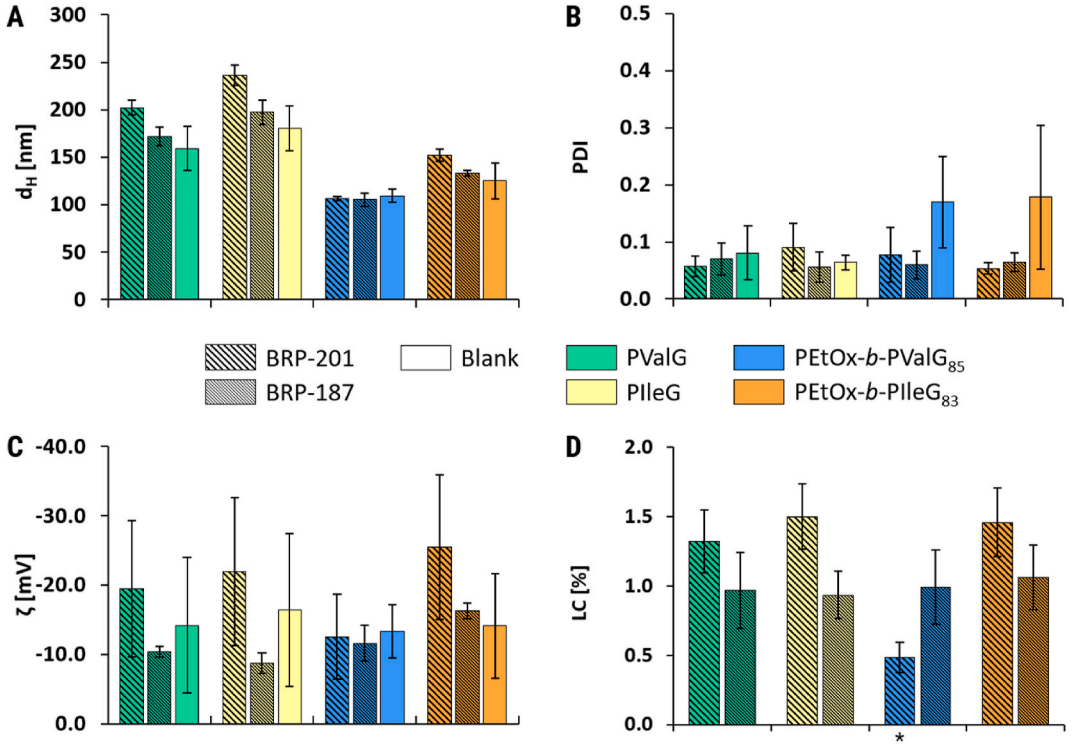

Fig. 5. Particle characteristics: (**A**) Z-average (d_H) values of the purified, lyophilized, and resuspended nanoparticles obtained by DLS measurements with the corresponding PDI values (**B**). (**C**) Zeta potential values of the nanoparticles measured by ELS. (**D**) Drug loading of the nanoparticles determined by UV–Vis measurements of the BRP-187 and BRP-201 at 316 nm, herein displayed as loading capacity LC [%]. *Additional purification step *via* filtration. Results are means n = 3 ± SD.

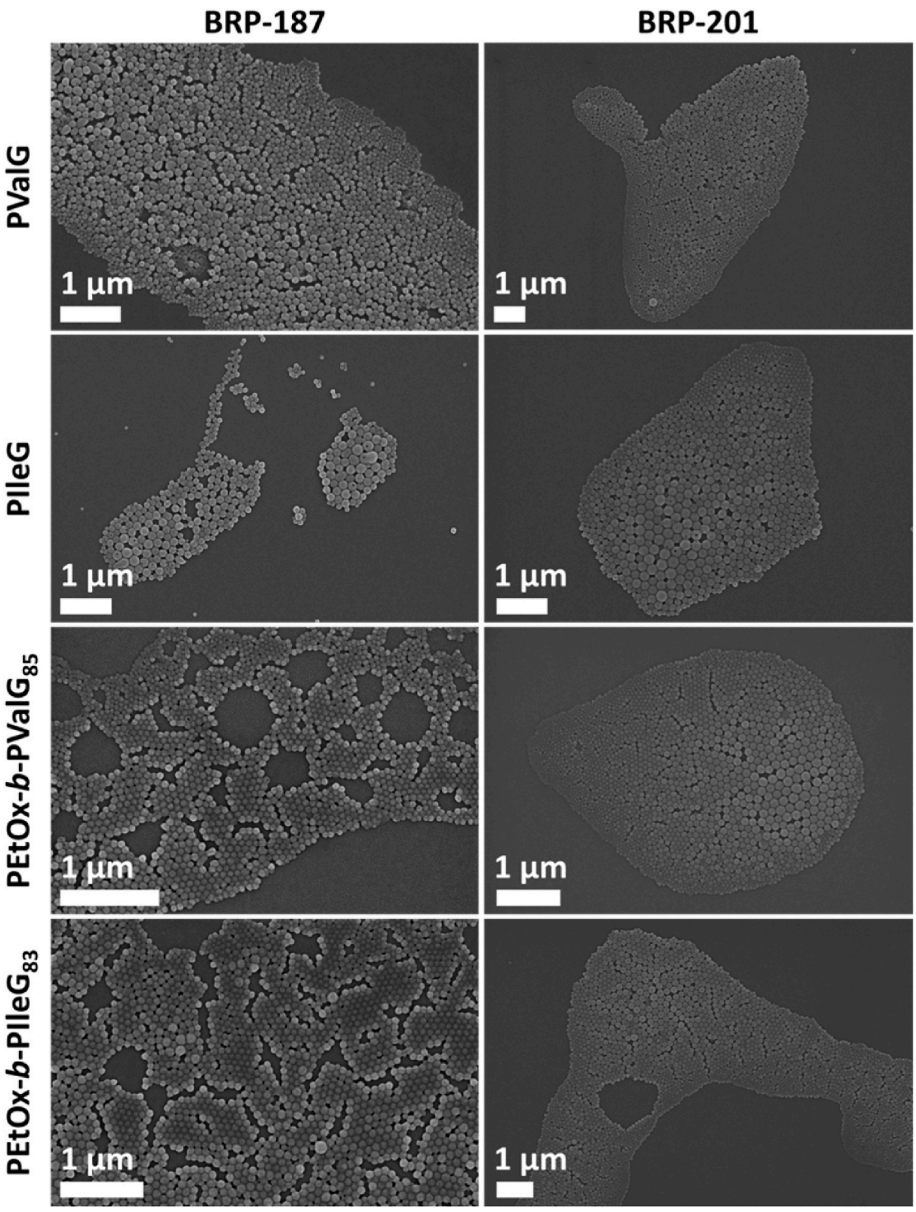

Fig. 6. Images of the purified BRP-187 and BRP-201 loaded nanoparticles obtained *via* Scanning electron microscopy analysis.

S10c) [47]. Similar to the unloaded nanoparticles prepared with surfactant, the zeta potential did not follow a clear trend regarding the presence of the PEtOx block.

SEM measurements, which were used as quality control to exclude the formation of API precipitates, confirmed the formation of uniform, spherical nanoparticles (Fig. 6). Non-encapsulated drug would form free drug precipitates visible in SEM as oblong, non-spherical sub-structures [5,6]. Such structures were absent in most of the formulations, confirming that both APIs were encapsulated into the nanoparticles. Free drug precipitates were only found in the SEM images of **PEtOx-*b*-P-ValG$_{85}$** revealing the lower encapsulation potential of the polymer for BRP-201 (Fig. S10). An additional purification step by filtration to remove the drug precipitates explains the decreased LC value of those nanoparticles (Fig. 5). In summary, all investigated nanoparticle systems were capable to encapsulate both APIs without revealing substantial differences regarding their properties compared to the blank nanoparticles.

3.3.3. *Uptake studies*

The investigated PEAs were, thus, principally capable of forming biocompatible nanoparticles that are stable, yet biodegradable. Additionally, those could also be loaded with different APIs. Their uptake into cells is furthermore crucial for their application. The particle uptake in HEK293 (WT) cells and human monocyte-derived macrophages was investigated by live cell confocal imaging. In order to enable the monitoring of the nanoparticles, the API BRP-187 was labeled with the fluorescent dye DY481XL-NH$_2$ (Scheme S11, Fig. S11). The dye-labeled BRP-187 (fluo-BRP-187) was subsequently encapsulated in all four systems, whereby the success of the encapsulation was proven by fluorescence measurements (Table S12, Figs. S12a and S12b). According to the DLS data, the nanoparticles featured sizes in the same range as the unlabeled nanoparticles (Table S12). During incubation of the various nanoparticles with HEK293 (WT) cells, live cell confocal imaging revealed an increasing fluorescent signal within the cells revealing an accumulated uptake of all particle systems within 5 h (Fig. S13a). Additionally, the uptake of valine-based nanoparticles **PValG** and

PEtOx-*b*-PValG$_{85}$ loaded with fluo-BRP-187 was studied in M1 macrophages over a period of 14 h using the same live cell confocal imaging procedure, but with a larger field of view (Fig. S13b). For both particle systems, a continuous uptake was observed while the cells proliferated and migrated over the whole observation period. Overall, no clear difference for the PEtOxylated nanoparticles was observed compared to the nanoparticles prepared from the homopolymers. However, the uptake studies demonstrated the internalization of all nanoparticles in general without producing obvious sings of cytotoxicity, such as cell detachment, reduced proliferation, cell death or cell lysis. This is also in agreement with literature where a fast uptake is described for polymeric nanoparticles with a negative zeta potential [48].

3.3.4. *Cell-based bioactivity studies*

BRP-187 and BRP-201 are potent agents for the reduction of pro-inflammatory 5-LOX-mediated leukotrienes by FLAP inhibition. Here, we evaluated the ability of the API-loaded nanoparticles to inhibit 5-LOX product formation in human neutrophils due to their high expression of the 5-LOX helper protein FLAP [49]. Furthermore, the API-loaded nanoparticles were tested in human whole blood due to its high abundance of neutrophils. All nanoparticles (BRP-187 and BRP-201 loaded) suppressed the FLAP-dependent formation of pro-inflammatory 5-LOX products in neutrophils as compared to the blank nanoparticles (Fig. 7 and Fig. S14).

The BRP-201-loaded nanoparticles prepared from the homopolymers, in particular those from **PValG**, performed similarly as the PLGA nanoparticles, which is in accordance with their alike degradation behavior (Fig. 3). The **PEtOx-*b*-PValG$_{85}$** and **PEtOx-*b*-PIleG$_{83}$** nanoparticles loaded with BRP-201 revealed the highest efficacy, even surpassing the loaded PLGA nanoparticles (Fig. 7). Since the same concentration of API was initially applied for all particle systems, the differences of the inhibition are explained by an altered interaction of the API with the carrier material. In order to inhibit FLAP, the nanoparticles must have released the API by the time the stimulus Ca^{2+}-ionophore A23187 is added so that the API is effectively available for FLAP inhibition in the first place. A closer look at the degradation studies and the t_{50} values demonstrated rapid particle degradation for the **PEtOx-*b*-PValG$_{85}$**, **PEtOx-*b*-PIleG$_{83}$**, and **PValG** nanoparticles, which consequently led to a fast and efficient API release. In contrast, the **PIleG** nanoparticles required significantly longer and more enzyme to be degraded and, thus, obviously could not deliver the API as efficiently. Parallel investigations of the toxicity of the nanoparticles showed that the viability of the neutrophils remained unaffected by using both the unloaded and loaded nanoparticles (Fig. 7B and Fig. S7C). Thus, an undesired influence on the inhibition of FLAP due to cytotoxicity was excluded. Similar trends in the 5-LO product suppression were also observed for the BRP-187 loaded nanoparticles, but to a lower extent (**Fig. S14**).

Further bioactivity studies were performed with valine-based samples with BRP-187 and all four polymers with BRP-201 in human whole blood (Fig. 7 and Fig. S14). Many FLAP inhibitors fail to suppress 5-LOX product formation due to their strong plasma protein binding tendency. None of the investigated particle systems, neither PEA- nor PLGA-based, led to a significant reduction in LTB_4 or even PGE_2 production in whole blood stimulated with *S. aureus*-conditioned medium for 90 min. Nevertheless, a tendency in LTB_4 suppression was observed for **PEtOx-*b*-PValG$_{85}$** and **PEtOx-*b*-PIleG$_{83}$** (Fig. 7C). Inefficient inhibition of LTB_4 formation in whole blood was also observed for PLGA in previous studies [6]. This might be partly due to an undesired rapid degradation of the nanoparticles *in vitro*. Release of the API may lead to strong plasma protein binding before its cellular uptake and the API being unable to unfold its full effectiveness. Therefore, further optimization of the particle systems is required in the future. To further improve efficiency in human blood, both PEtOx block length and density (*via* co-formulations) can be varied to achieve modified stability and degradation profiles.

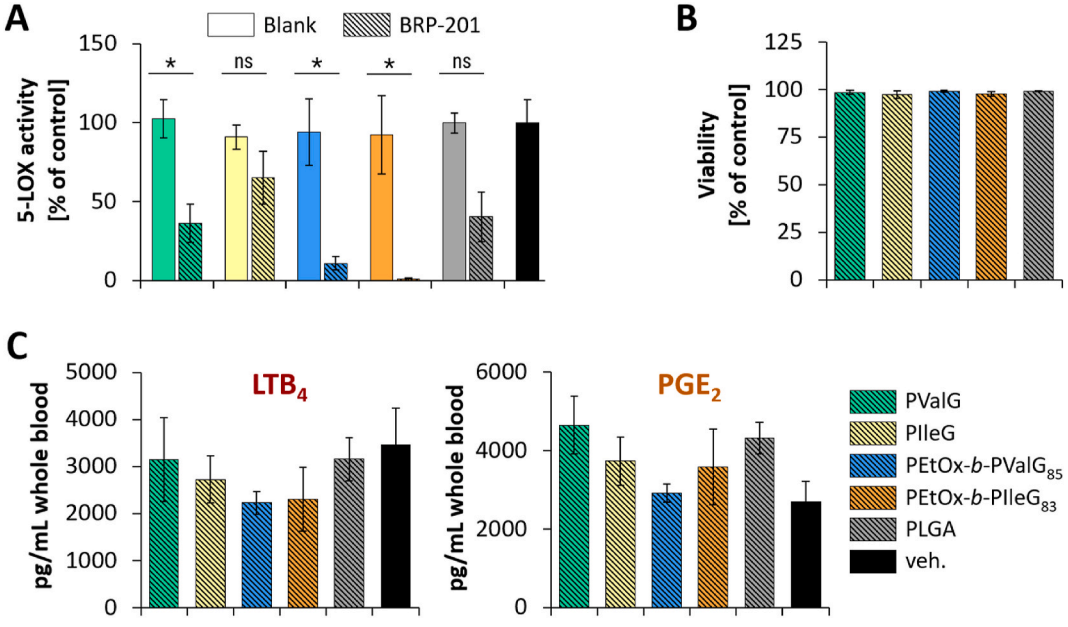

Fig. 7. Inhibition of pro-inflammatory lipid mediators by encapsulated BRP-201 in nanoparticles formed with different polymers. (**A**) Neutrophils were preincubated with nanoparticles (encapsulated with BRP-201 at 0.1 μM or without) for 1 h at 37 °C and then stimulated with 2.5 μM A23187. After 10 min, the reaction was stopped, and 5-LOX products were extracted *via* solid phase extraction (SPE) and analyzed with HPLC. Values are given as 5-LOX products (LTB_4, *trans*-LTB_4, *epi*-trans-LTB_4 and 5-HETE) in percentage (%) of control. Results are means ±standard error of mean, n = 3; Data were log-transformed for statistical analysis; *$p < 0.05$, multiple paired *t*-test. (**B**) For determination of cytotoxicity, LDH release were monitored after 60 min, results are shown as means ±standard error of mean in bar charts, n = 3. (**C**) Freshly withdrawn whole blood from human donors was preincubated with vehicle (veh., 0.1 % PBS), nanoparticles (loaded with BRP-201 at 10 μM) for 5 h at 37 °C and then stimulated with 3 % *S. aureus*-conditioned medium for 90 min. The reaction was stopped, and LTB_4 and PGE_2 were extracted *via* SPE and analyzed with UPLC-MS-MS. Values are given as pg/mL whole blood. Results are means ± standard error of mean n = 3.

4. Conclusions

Initial high-throughput formulations demonstrated the suitability of valine- and isoleucine-based PEAs to form nanoparticles. Systematic testing of co-formulations of the homopolymers with the different PEtOx block copolymers in defined ratios was performed. This unveiled the potential of particle size adjustments through the material selection itself, at otherwise similar conditions. Based on the lipophilic character of the selected APIs (BRP-187 and BRP-201), the **PValG** and **PIleG** homopolymers as well as the most hydrophobic copolymers **PEtOx-*b*-PValG$_{85}$** and **PEtOx-*b*-PIleG$_{83}$** were selected for further encapsulation studies. The calculations performed *via* atomistic molecular dynamics simulations suggested the miscibility of the investigated polymers and APIs, which was verified experimentally. Both drugs could be encapsulated in all four polymer nanoparticles by nanoprecipitation. Neither empty nor loaded nanoparticles revealed toxicity, their stability was confirmed and they did not tend to aggregate. The nanoparticles were biodegradable by proteinase K, whereby kinetic differences were evident between the four systems, which allows even better tunability of the carrier properties. It was verified that nanoparticles are taken up by HEK293 (WT) cells as well as macrophages and that the loaded nanoparticles were able to reduce the FLAP-dependent 5-LOX product formation as desired for an anti-inflammatory drug carrier system. The strongest effects were observed for the BRP-201-loaded nanoparticles. In particular, the two **PEtOx-*b*-PValG$_{85}$** and **PEtOx-*b*-PIleG$_{83}$** formulations were even more effective than the PLGA control sample in their inhibitory activity. Overall, it was shown that PEAs are promising alternative polymers to the conventionally used PLGA, in particular in combination with the PEtOx block attached as an alternative to the frequently used PEG. Future investigations will focus on optimizing the PEtOx-PEA carriers to ensure that their performance improves in whole blood and they can ultimately be applied *in vivo*, thus enabling their transfer into therapy-relevant applications.

CRediT authorship contribution statement

Mira Behnke: Conceptualization, Data curation, Writing - original draft. **Antje Vollrath:** Conceptualization, Writing - review & editing. **Philipp Dahlke:** Investigation. **Francisco Páez Larios:** Investigation. **Mingzhe Chi:** Investigation. **Ekaterina Tsarenko:** Investigation. **Paul M. Jordan:** Investigation. **Christine Weber:** Methodology, Writing - review & editing. **Michael Dirauf:** Investigation. **Justyna Anna Czaplewska:** Investigation. **Baerbel Beringer-Siemers:** Investigation. **Steffi Stumpf:** Investigation. **Carolin Kellner:** Investigation. **Christian Kretzer:** Investigation. **Stephanie Hoeppener:** Supervision, Writing - review & editing. **Ivo Nischang:** Supervision, Writing - review & editing. **Marek Sierka:** Supervision, Writing - review & editing. **Christian Eggeling:** Supervision, Writing - review & editing. **Oliver Werz:** Supervision, Writing - review & editing. **Ulrich S. Schubert:** Supervision, Writing - review & editing.

Declaration of competing interest

The authors declare no competing financial interest.

Data availability

Data will be made available on request.

Acknowledgement

The authors acknowledge the support of Deutsche Forschungsgemeinschaft (DFG, German Research Foundation, project number 316213987, SFB 1278, projects A01, A04, A06, and Z01). I.N. acknowledges funding by the DFG – 471397362. The UHPLC was funded by the DFG – 438688627. The SEM facilities of the Jena Center for Soft Matter (JCSM) were established with a grant from the DFG. We thank Dorottya Koppenhagen for the culture of our HEK293 cells and the Microverse Imaging Centre and Aurélie Jost/Patrick Then for providing microscope facility support for data acquisition and data analysis. The LSM 980 used for our live-cell imaging experiments was funded by the Free State of Thuringia with the grant number 2019 FGI 0001. The Microverse Imaging Centre is funded by the DFG under Germany's Excellence Strategy – EXC 2051 – Project-ID 390713860.

Appendix A. Supplementary data

Supplementary data to this article can be found online at https://doi.org/10.1016/j.mtchem.2023.101848.

References

[1] B. Begines, T. Ortiz, M. Pérez-Aranda, G. Martínez, M. Merinero, F. Argüelles-Arias, A. Alcudia, Nanomaterials 10 (2020) 1403.
[2] M. Behnke, C.T. Holick, A. Vollrath, S. Schubert, U.S. Schubert, in: M. Schaefer-Korting, U.S. Schubert (Eds.), Handbook of Experimental Pharmacology, Springer Berlin Heidelberg, Berlin, Heidelberg, 2023, pp. 1–24.
[3] C. Englert, J.C. Brendel, T.C. Majdanski, T. Yildirim, S. Schubert, M. Gottschaldt, N. Windhab, U.S. Schubert, Prog. Polym. Sci. 87 (2018) 107–164.
[4] H.O. Alsaab, F.D. Alharbi, A.S. Alhibs, N.B. Alanazi, B.Y. Alshehri, M.A. Saleh, F. S. Alshehri, M.A. Algarni, T. Almugaiteeb, M.N. Uddin, R.M. Alzhrani, Pharmaceutics 14 (2022) 2728.
[5] M. Behnke, A. Vollrath, L. Klepsch, B. Beringer-Siemers, S. Stumpf, J. A. Czaplewska, S. Hoeppener, O. Werz, U.S. Schubert, Polymers 12 (2020) 2751.
[6] C. Kretzer, B. Shkodra, P. Klemm, P.M. Jordan, D. Schroder, G. Cinar, A. Vollrath, S. Schubert, I. Nischang, S. Hoeppener, S. Stumpf, E. Banoglu, F. Gladigau, R. Bilancia, A. Rossi, C. Eggeling, U. Neugebauer, U.S. Schubert, O. Werz, Cell. Mol. Life Sci. 79 (2021) 40.
[7] I. Muljajew, M.Z. Chi, A. Vollrath, C. Weber, B. Beringer-Siemers, S. Stumpf, S. Hoeppener, M. Sierka, U.S. Schubert, Eur. Polym. J. 156 (2021), 110606.
[8] M. Winnacker, B. Rieger, Polym. Chem. 7 (2016) 7039–7046.
[9] N. Brunacci, A.T. Neffe, C. Wischke, T. Naolou, U. Noechel, A. Lendlein, J. Contr. Release 301 (2019) 146–156.
[10] T.F. Burton, J. Pinaud, O. Giani, Macromolecules 53 (2020) 6598–6607.
[11] P.J.A. in, t Veld, P.J. Dijkstra, J.H. van Lochem, J. Feijen, Makromol. Chem. 191 (1990) 1813–1825.
[12] Y. Feng, D. Klee, H. Keul, H. Hoecker, Macromol. Chem. Phys. 201 (2000) 2670–2675.
[13] J. Liu, Y. Xiao, C. Allen, J. Pharmaceut. Sci. 93 (2004) 132–143.
[14] M. Dirauf, I. Muljajew, C. Weber, U.S. Schubert, Prog. Polym. Sci. 129 (2022), 101547.
[15] K. Pagar, P. Vavia, Sci. Pharm. 81 (2013) 865–888.
[16] K.P. Pagar, P.R. Vavia, Ther. Deliv. 4 (2013) 553–565.
[17] K.P. Pagar, P.R. Vavia, Pharmaceut. Dev. Technol. 19 (2014) 385–394.
[18] K. Knop, R. Hoogenboom, D. Fischer, U.S. Schubert, Angew. Chem. Int. Ed. 49 (2010) 6288–6308.
[19] X. Yao, C. Qi, C. Sun, F. Huo, X. Jiang, Nano Today 48 (2023), 101738.
[20] T.T. Hoang Thi, E.H. Pilkington, D.H. Nguyen, J.S. Lee, K.D. Park, N.P. Truong, Polymers 12 (2020) 298.
[21] M. Dirauf, A. Erlebach, C. Weber, S. Hoeppener, J.R. Buchheim, M. Sierka, U. S. Schubert, Macromolecules 53 (2020) 3580–3590.
[22] L. Shi, J. Zhang, M. Zhao, S. Tang, X. Cheng, W. Zhang, W. Li, X. Liu, H. Peng, Q. Wang, Nanoscale 13 (2021) 10748–10764.
[23] R. Ferrari, M. Sponchioni, M. Morbidelli, D. Moscatelli, Nanoscale 10 (2018) 22701–22719.
[24] Z.T. Gür, B. Çalışkan, U. Garscha, A. Olgaç, U.S. Schubert, J. Gerstmeier, O. Werz, E. Banoglu, Eur. J. Med. Chem. 150 (2018) 876–899.
[25] U. Garscha, S. Voelker, S. Pace, J. Gerstmeier, B. Emini, S. Liening, A. Rossi, C. Weinigel, S. Rummler, U.S. Schubert, G.K. Scriba, E. Celikoglu, B. Caliskan, E. Banoglu, L. Sautebin, O. Werz, Biochem. Pharmacol. 119 (2016) 17–26.
[26] B. Shkodra-Pula, C. Kretzer, P.M. Jordan, P. Klemm, A. Koeberle, D. Pretzel, E. Banoglu, S. Lorkowski, M. Wallert, S. Hoppener, S. Stumpf, A. Vollrath, S. Schubert, O. Werz, U.S. Schubert, J. Nanobiotechnol. 18 (2020) 73.
[27] E. Banoglu, E. Celikoglu, S. Volker, A. Olgac, J. Gerstmeier, U. Garscha, B. Caliskan, U.S. Schubert, A. Carotti, A. Macchiarulo, O. Werz, Eur. J. Med. Chem. 113 (2016) 1–10.
[28] B. Shkodra-Pula, C. Grune, A. Traeger, A. Vollrath, S. Schubert, D. Fischer, U. S. Schubert, Int. J. Pharm. 566 (2019) 756–764.
[29] S. Spek, M. Haeuser, M.M. Schaefer, K. Langer, Appl. Surf. Sci. 347 (2015) 378–385.
[30] E. Tsarenko, U.S. Schubert, I. Nischang, Anal. Chem. 95 (2023) 565–569.
[31] A.O. Kasimova, G.M. Pavan, A. Danani, K. Mondon, A. Cristiani, L. Scapozza, R. Gurny, M. Moeller, Chimia 67 (2013) 87.
[32] L. Huynh, J. Grant, J.C. Leroux, P. Delmas, C. Allen, Pharm. Res. (N. Y.) 25 (2008) 147–157.
[33] I. Muljajew, A. Erlebach, C. Weber, J.R. Buchheim, M. Sierka, U.S. Schubert, Polym. Chem. 11 (2020) 112–124.

[34] A. Erlebach, I. Muljajew, M. Chi, C. Bueckmann, C. Weber, U.S. Schubert, M. Sierka, Adv. Theory Simul. 3 (2020), 2000001.
[35] C. Kretzer, P.M. Jordan, K.P.L. Meyer, D. Hoff, M. Werner, R.K. Hofstetter, A. Koeberle, A. Cala Peralta, G. Viault, D. Seraphin, P. Richomme, J.-J. Helesbeux, H. Stuppner, V. Temml, D. Schuster, O. Werz, Biochem. Pharmacol. 195 (2022), 114825.
[36] O. Werz, E. Bürkert, B. Samuelsson, O. Radmark, D. Steinhilber, Blood 99 (2002) 1044–1052.
[37] M. Werner, P.M. Jordan, E. Romp, A. Czapka, Z. Rao, C. Kretzer, A. Koeberle, U. Garscha, S. Pace, H.E. Claesson, C.N. Serhan, O. Werz, J. Gerstmeier, Faseb. J. 33 (2019) 6140–6153.
[38] J. Kimmig, T. Schuett, A. Vollrath, S. Zechel, U.S. Schubert, Adv. Sci. 8 (2021), 2102429.
[39] Q. Liu, C. Cai, C.M. Dong, J. Biomed. Mater. Res., Part A 88A (2009) 990–999.
[40] L. Wang, S.-Y. Li, W. Jiang, H. Liu, J.-X. Dou, X.-Q. Li, Y.-C. Wang, ACS Appl. Mater. Interfaces 12 (2020) 32312–32320.
[41] G. Cinar, J.I. Solomun, P. Mapfumo, A. Traeger, I. Nischang, Anal. Chim. Acta 1205 (2022), 339741.
[42] C. He, Y. Hu, L. Yin, C. Tang, C. Yin, Biomaterials 31 (2010) 3657–3666.
[43] S.K. Sahoo, J. Panyam, S. Prabha, V. Labhasetwar, J. Contr. Release 82 (2002) 105–114.
[44] A.C. Fonseca, M.H. Gil, P.N. Simões, Prog. Polym. Sci. 39 (2014) 1291–1311.
[45] P. Ranganathan, C.-W. Chen, S.-P. Rwei, Y.-H. Lee, S.K. Ramaraj, Polym. Degrad. Stabil. 181 (2020), 109323.
[46] A.B. Beklemishev, M.B. Pykhtina, Y.M. Kulikov, T.N. Goryachkovskaya, D. V. Bochkov, S.V. Sergeeva, A.R. Vasileva, V.P. Romanov, D.S. Novikova, S. E. Peltek, Vavilov J. Genet. Breed. 25 (2021) 882–888.
[47] O. Taratula, B.S. Doddapaneni, C. Schumann, X. Li, S. Bracha, M. Milovancev, A.W. G. Alani, O. Taratula, Chem. Mater. 27 (2015) 6155–6165.
[48] A. Musyanovych, J. Dausend, M. Dass, P. Walther, V. Mailänder, K. Landfester, Acta Biomater. 7 (2011) 4160–4168.
[49] N.C. Gilbert, M.E. Newcomer, O. Werz, Biochem. Pharmacol. 193 (2021), 114759.